AIAA JOURNAL
Vol. 41, No. 12, December 2003

Large-Scale Structures in a Compressible Mixing Layer over a Cavity

J. Poggie*
U.S. Air Force Research Laboratory, Wright–Patterson Air Force Base, Ohio 45433-7512
and
A. J. Smits†
Princeton University, Princeton, New Jersey 08544-5263

An experimental study was made of a flow in which a turbulent boundary layer separates at a backward-facing step, forms a free shear layer over a cavity, and reattaches on a ramp downstream. Accurate characterization of the mixing layer turbulence is important given the strong link between large-scale organized structures and intense unsteadiness at reattachment found in our previous study of this flow (Poggie, J., and Smits, A. J., "Shock Unsteadiness in a Reattaching Shear Layer," *Journal of Fluid Mechanics*, Vol. 429, 2001, pp. 155–185). To this end, detailed flow visualization experiments were carried out in the self-similar portion of the turbulent mixing layer at a nominal convective Mach number of 1.1. The flow visualization technique was based on Rayleigh scattering from nanometer-scale contaminant particles present in the freestream flow. The interface marked by the vaporization of the particles revealed the large-scale organized turbulence structures in the mixing layer. Quantitative measures of the length scale, orientation, and speed of organized structures were derived from the flow visualization data, and were found to agree well with conventional point-probe measurements. As has been found in other studies of planar mixing layers, the measured convection velocity varied moderately along the transverse direction, and the corresponding convective Mach number differed from the prediction of the isentropic model. The present results, along with previously published probe surveys, demonstrate that the flow over the cavity is essentially equivalent to a standard planar mixing layer flow, and thus forms a well-characterized initial condition for the reattachment flow downstream. In combination with our previous study, the present results add insight into cavity flow unsteadiness for the case where the driving mechansim is related to broad-band turbulent fluctuations, rather than discrete acoustic resonances.

Introduction

Background

A REGION of separated, supersonic flow must often be tolerated on the surface of an air vehicle due to the compromises inherent in the design process. Examples include separation caused by rapid compression, such as the root vortex at the base of a fin or deflected flap, as well as separation due to a sudden change in geometry, such as a cavity flame holder or an open bay for store release. These flow regions are typically turbulent, with intense, large-scale unsteadiness, and may result in severe aircraft fatigue loading.

In confined flows, for example, flow over a rectangular cavity, the dominant cause of the unsteadiness can be a resonant oscillation caused by acoustic waves traveling upstream in the subsonic part of the flow.[1,2] However, for less confined flows, and in general for higher Mach numbers, the primary mechanism for the unsteadiness may be the response of the separated region to organized structures in the incoming turbulent flow.[3–5] This behavior is illustrated nicely in time-resolved flow visualization of separated, supersonic flows.[4–7]

The present paper reports part of a study[8] of a Mach 2.9 flow in which a turbulent boundary layer separates at a backward-facing step, forming a free shear layer that reattaches on a ramp downstream (Fig. 1). As part of the study reported in a previous paper,[5] artificial disturbances were introduced into the flow through steady air injection in the vicinity of separation to examine the influence of disturbances originating in the incoming shear layer. The effect on the reattachment shock system was dramatic: The intensity of the pressure fluctuations and the amplitude of the shock motion increased substantially, and power spectra of the pressure fluctuations showed a distinct shift to lower frequency. A very interesting observation in that work was that the spectra collapsed onto a common curve in nondimensional coordinates based on length and velocity scales for the shear layer near reattachment.

Figure 2 shows some of these results, the autospectra of the fluctuating pressure signal just downstream of mean reattachment (82.6 mm up the ramp). The data are seen to have a broadband energy content, with no prominent peaks. Air injection is seen to shift the dimensional spectrum (Fig. 2a) to higher values, reflecting the increase in the intensity of pressure fluctuations. Analogous features in the spectra are also seen to be shifted to lower frequency in the air injection case. Note, in particular, the shift to lower frequency of the "knee" in the spectrum, which is present near 2 kHz in the undisturbed flow data.

Figure 2b shows the spectral data plotted in normalized form. The frequency was nondimensionalized by a length scale δ_c, derived from two-point cross correlations of flow visualization obtained near reattachment, and by a velocity scale U_c, derived from cross correlations of the pressure fluctuations on the ramp. The spectrum was divided by the mean square fluctuating pressure $\overline{p'^2}$ and the timescale δ_c/U_c. The data collapse well. In particular, nondimensionalizing the frequency causes the knees in the spectra to line up.

Given the importance of the shear layer turbulence in driving reattachment unsteadiness, as well as the intrinsic importance of large-scale organized structures in mixing layer growth, a detailed study of the flow above the cavity is presented in this paper. The large-scale structures in the mixing layer are characterized using quantitative measures derived from flow visualization data. The length scale, orientation, and speed of the structures were measured and compared to the results of other studies.

Received 9 April 2003; revision received 18 August 2003; accepted for publication 18 August 2003.

*Research Aerospace Engineer, Computational Sciences Center, Air Vehicles Directorate. Senior Member AIAA.
†Professor, Department of Mechanical and Aerospace Engineering. Fellow AIAA.

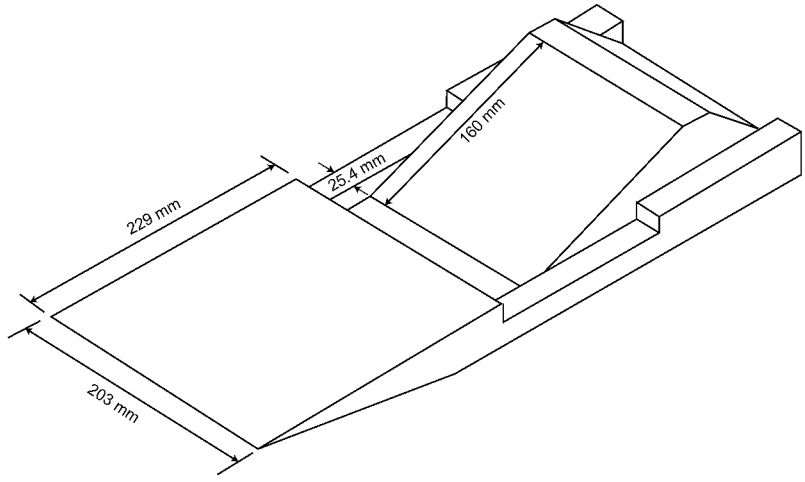

a) Diagram of the experimental model

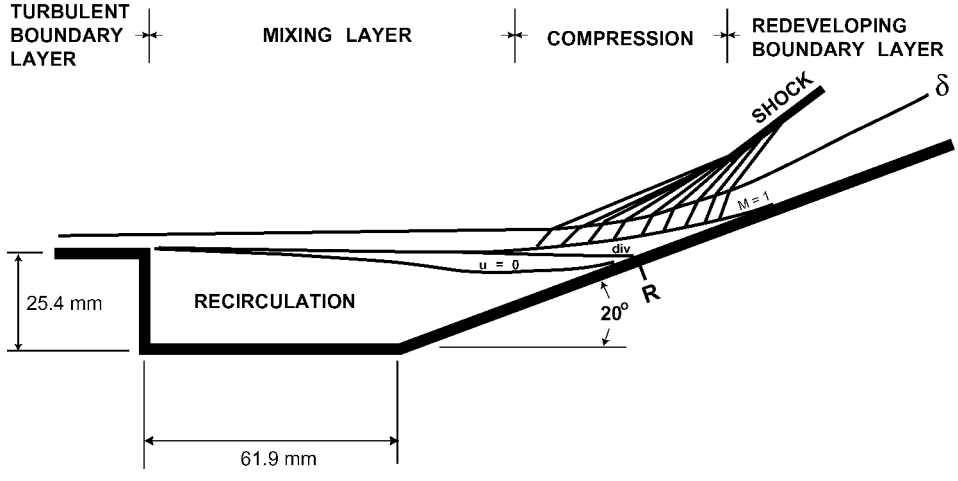

b) Cross section of the mean flowfield: R, reattachment location; δ, boundary layer/shear layer edge; $M = 1$, sonic line; div, dividing streamline; $u = 0$, boundary of recirculating region

Fig. 1 Experimental configuration (adapted from Baca[22]).

Free Shear Layers

In incompressible flow, studies of the nonlinear stages of transition have uncovered the origin of some of the coherent structures observed in mixing layers.[9–11] The Kelvin–Helmholtz instability introduces uniform spanwise vortices into an initially laminar shear layer. Disturbances in the flow create small wrinkles in the spanwise vortex filaments, which are amplified by vortex induction. The filaments are stretched along the principal direction of strain in the vicinity of the free stagnation point between two spanwise vortices. The newly formed quasi-streamwise vortices in turn induce additional undulations into the spanwise vortices, and the vortex system grows progressively more complicated as it convects downstream. Additional complexity is introduced through pairing, tearing, and amalgamation. Farther downstream in the fully turbulent portion of a mixing layer, organized structures similar to the spanwise and streamwise vortices exist in the flow.[9] These phenomena are also observed experimentally in flows with relatively weak compressibility effects.[12]

In compressible flow, oblique disturbances, rather than spanwise disturbances, are most unstable. Correspondingly, oblique, three-dimensional structures are observed experimentally in turbulent mixing layer flows with strong compressibility effects.[12–14]

To characterize the compressibility effects felt by organized structures in a mixing layer, Bogdanoff[15] introduced a Mach number based on the velocity of a structure relative to the freestream flow. The convective Mach number is defined as follows:

$$M_{ci} = |U_i - U_c|/a_i \tag{1}$$

where U_c is the speed of coherent structures in the flow, whereas U_i is the flow speed and a_i is the sound speed in the freestream on side $i = 1, 2$ of the mixing layer.

An estimate of the convective Mach number can be derived from a simple isentropic model.[15,16] According to this model, in a reference frame moving at the convection speed of the large-scale motions U_c, the flow is approximately steady if the structures grow slowly compared to the time it takes a fluid particle to travel through them. The streamline pattern in this reference frame looks something like Fig. 3, after Papamoschou and Roshko.[16]

Fluid from the two streams meets at the saddle point, where the velocity is zero. Assume that the fluid from each stream decelerates isentropically to rest at the saddle point, so that the pressure at the saddle point is equal to the stagnation pressure in each of the freestreams. If the shear layer is thin compared to its radius of curvature and the distance from its origin, then the static pressures in the two freestreams will also be equal. Thus, we can equate the ratio of total to static pressure for the two streams. If the specific heat ratios of the two streams are equal, the equal pressure ratios imply that the convective Mach numbers for the two streams are equal, leading to the following expression for the convection velocity:

$$U_c = \frac{a_2 U_1 + a_1 U_2}{a_2 + a_1} \tag{2}$$

Substituting Eq. (2) back into Eq. (1) gives the form for the convective Mach numbers predicted by the isentropic model:

$$M_{c1} = M_{c2} = (U_1 - U_2)/(a_1 + a_2) \tag{3}$$

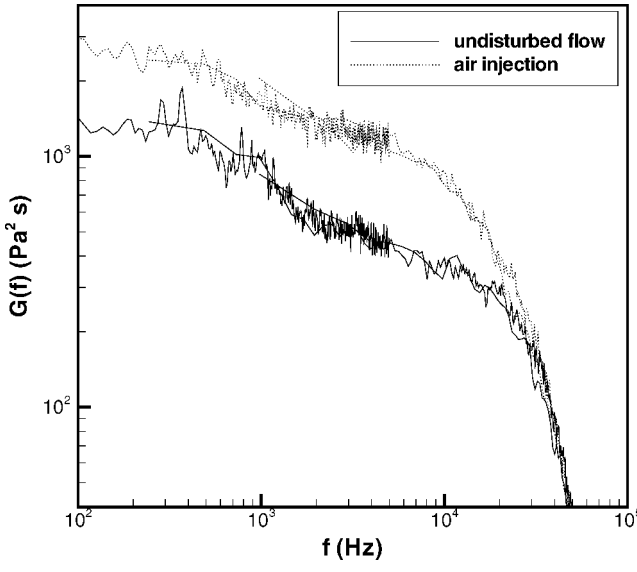

a) Dimensional spectrum

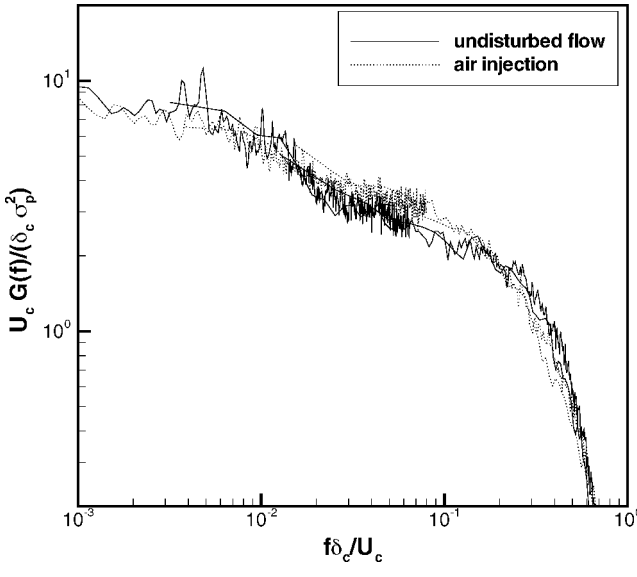

b) Nondimensional spectrum

Fig. 2 Autospectra of wall pressure fluctuations just downstream of reattachment.

For the present paper, we will call this parameter the nominal convective Mach number.

When the growth rate of a free shear layer in compressible flow is normalized by the incompressible flow value at the same velocity and density ratio, the data more or less fall onto a single curve that is a function of the nominal convective Mach number.[16,17] The normalized growth rate decreases with increasing nominal convective Mach number from the incompressible flow value of 1.0 to an asymptotic value in the range 0.2–0.4 for supersonic convective Mach number. This reduction in growth rate is believed to be related to energy loss from the flow turbulence through radiated sound and through energy dissipation in shocklets (see Ref. 18, Sec. 6.3).

Experimental data, however, show that the convection velocity and convective Mach number as defined by Eq. (1) are not necessarily constant across a mixing layer,[12] and the measured convective Mach number may differ from the nominal convective Mach number defined in Eq. (3).[19] In the present experimental program, measurements of the convective Mach number have been made in a flow with a relatively high degree of compressibility [$M_c = 1.1$ from Eq. (1), with $U_1 = U_\infty$ and $U_2 = 0$] and will be compared with available data from other flows.

Table 1 Properties of turbulent boundary layer in the vicinity of the backward-facing step

Property	Value
θ	0.17 mm
δ	2.9 mm
Π	0.76
M_e	2.90 ± 0.01
Re_θ	1.0×10^4
Re_δ	1.9×10^5
C_f	1.4×10^{-3}

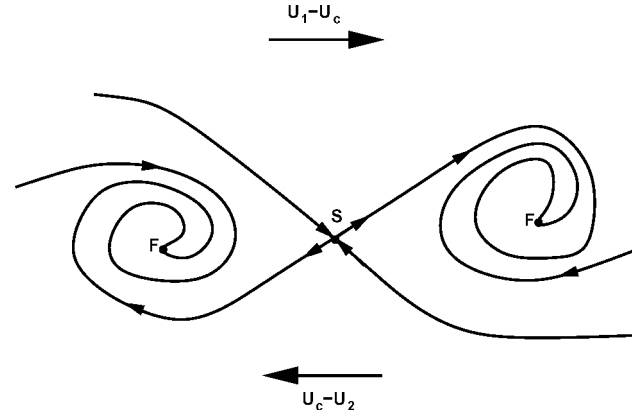

Fig. 3 Simplified streamline pattern of free shear layer structures in a convective reference frame: F, focus and S, saddle (after Papamoschou and Roshko[16]).

Experimental Facilities and Methods

The experiments were carried out in the Princeton University Mach 3 blowdown wind tunnel.[20,21] The pressure in the settling chamber was maintained at 0.689 MPa ± 1% for all of the experiments described in this paper. In a typical 2-min run, the stagnation temperature was initially 290 K and dropped by about 8% over the run. Data were typically acquired in a 20-s window within the run (20 s at 10 Hz imaging rate gives 200 images), for a 1% drop in stagnation temperature. The stagnation temperature was recorded during each run, and the average value was used to reduce the data.

The experimental model was designed by Baca[22] and was mounted in the first test section of the wind tunnel (Fig. 1). The model consists of a wedge-shaped plate containing a cavity 25.4 mm deep, starting 228.6 mm downstream of the leading edge. A 20-deg ramp, 160.0 mm long, lies 61.9 mm downstream of the start of the cavity. When the plate is installed parallel to the freestream flow in the wind tunnel, the roof of the tunnel is 152.4 mm above the plate, and the plate spans the 203.2 mm width of the test section. To avoid interference from the side-wall boundary layers, the cavity and the ramp are inset by 25.4 mm on each side of the test section. The setup includes a step in the upper wall of the test section and provisions for flow under the model to avoid choking the wind tunnel.

An equilibrium turbulent boundary layer exists on the upper surface of the plate during a wind-tunnel run, forming the inlet boundary condition to the mixing layer flow.[22] In the freestream, the turbulence intensity is on the order of 1% and the Mach number is 2.9. Some of the parameters characterizing the boundary layer are listed in Table 1.

Because of the position of the ramp, the boundary layer separates at the backward-facing step with a minimal change in flow direction. The mean velocity profiles of the resulting free shear layer reach a self-similar condition at a distance downstream of the step equal to about 18 times the boundary-layer thickness at detachment. In this region, the shear layer has a growth rate that is in good agreement with data from other compressible, turbulent mixing layer experiments.[23] The nominal convective Mach number is about 1.1 for this flow.

A frequency-quadrupled Nd:YAG laser provided illumination at a wavelength of 266 nm for the flow visualization experiments. In

single-pulse mode, the laser fired at a rate of 10 Hz, delivering pulses with a duration of several nanoseconds. Typical energy outputs at 266 nm were in the range of 20–50 mJ per laser pulse. The laser could also be fired in double-pulse mode, in which a pair of closely spaced pulses (with the time delay adjustable between 15 and 60 μs) are delivered every 0.1 s. The energy per pulse was generally lower in this mode and tended to decrease with decreasing pulse spacing. A laser sheet was formed in the wind-tunnel test section using UV optics, and a double-intensified ITT charge integrated device camera oriented normal to the sheet recorded the scattered light. The camera alignment and field of view were determined by imaging a precision grid placed in the wind-tunnel test section aligned with the laser sheet.

To reduce the effects of laser sheet nonuniformity on the results, the images were preprocessed using a linear calibration procedure. For a detailed description of this procedure and some examples of the results, see Refs. 8 and 24. The analyses were repeated both with and without preprocessing, and the calibration was found to have only a moderate effect on the results. For example, the correlation contours showed a change in the characteristic length scale of no more than 10%.

The scattering particles are believed to be nanometer-scale clusters of water, carbon dioxide, or oxygen molecules that formed in the expansion process of the wind-tunnel nozzle.[25] The interface marked by the vaporization of the particles revealed large-scale organized turbulence structures in the outer part of the turbulent mixing layer. The interpretation of data obtained with this technique is addressed in detail in Ref. 26.

Single-Pulse Experiments

Qualitative Results

Single-pulse Rayleigh scattering experiments were carried out using laser sheets oriented in both horizontal and vertical planes. The location of the field of view in each of the experiments was situated within the region of the flow (between 58 and 89 mm downstream of the backward-facing step) where the shear layer mean velocity profiles have been found to be self-similar.[22,27]

The first set of single-pulse Rayleigh scattering experiments was carried out using a vertical laser sheet oriented along the centerline of the wind tunnel. The field of view was 23.0 mm wide by 17.2 mm high. The upstream edge of the field of view was located 56.1 mm downstream of the backward-facing step, and the bottom edge was located 17.6 mm above the floor of the cavity of the experimental model. The results of a pitot probe survey[22] in this region of the flow (a station 71 mm downstream of the step) indicate that the thickness of the undisturbed shear layer is $\delta = 10.6$ mm and that the height of the zero mean velocity line is $y_0 = 20.4$ mm. Thus, the field of view is 2.2δ wide by 1.6δ high and spans a range of nondimensional heights in the shear layer of $-0.26 \leq (y - y_0)/\delta \leq 1.36$.

Figure 4 shows a set of four instantaneous images of the flow. The flow direction in the freestream is from left to right. As seen in previous investigations of a Mach 2.9 turbulent boundary layer using Rayleigh scattering (Refs. 24 and 26), the images display a highly convoluted interface between the particle-free fluid in the mixing layer and the particle-laden fluid in the freestream. Organized structures, with a length scale on the order of 20% of the shear layer thickness and oriented at an angle of approximately 45 deg, are revealed in the profile of this interface. Weak shocks are often visible on the original video record of the experimental results. Images of these shocks are, unfortunately, difficult to reproduce in printed form.

A second set of single-pulse Rayleigh scattering images provided plan-view images of the shear layer (Fig. 5). A horizontal laser sheet was used, located at a height of 22.9 mm or $(y - y_0)/\delta = 0.32$ within the shear layer ($y_0 = 19.3$ mm and $\delta = 11.4$ mm at a station 76.2 mm downstream of the backward-facing step,[22] the center of the field of view). The field of view began 60 mm downstream of the backward-facing step, and the images were 43.4 mm wide by 32.5 mm high, or roughly 3.8δ by 2.9δ. The data are shown in Fig. 5 in a group of four images, and the predominant flow direction is from top to bottom in each image.

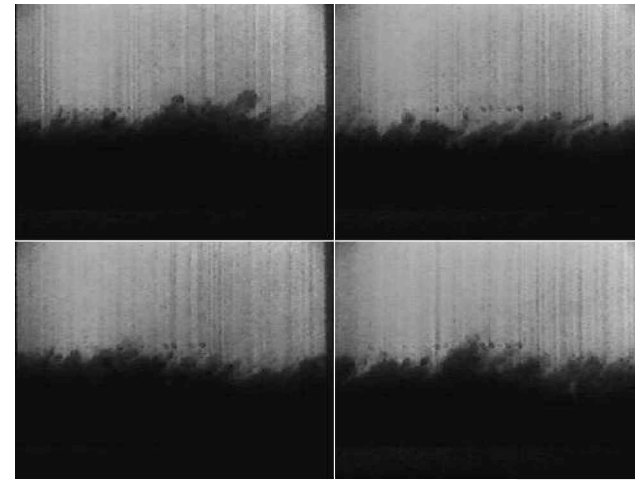

Fig. 4 Side-view Rayleigh scattering images of free shear layer.

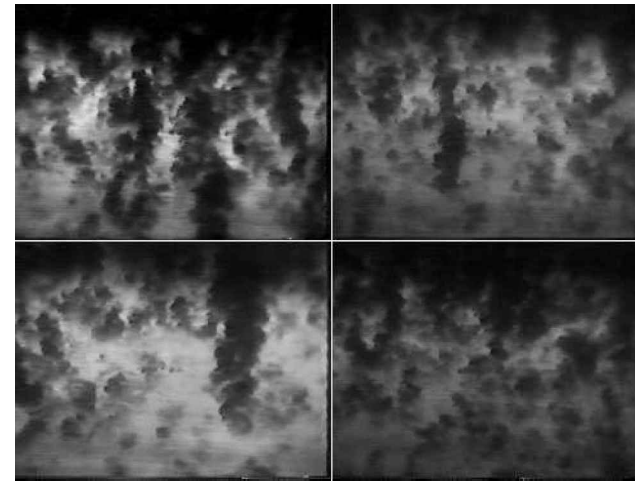

Fig. 5 Rayleigh scattering images of a horizontal plane through the free shear layer.

The dark structures are horizontal sections through the large-scale bulges seen in the side views of the shear layer. (Note that the upper edge of each image in Fig. 5 appears somewhat dark due to nonuniformity in the laser sheet that was too great for the calibration procedure to correct completely.) Some of the structures are highly elongated in the streamwise direction, but many have roughly the same length scale along both the spanwise and streamwise directions. The spanwise length scale of the structures at this height in the shear layer is between $\delta/4$ and $\delta/2$, whereas the streamwise length scale reaches up to 3δ.

Shear Layer Profiles

Figure 6 compares the normalized mean scattering intensity profile in the turbulent mixing layer to a mean density profile derived from probe measurements.[22] If there were no particle contaminants in the flow, and all of the collected light were due to molecular scattering, then these profiles would be expected to coincide. With the presence of particles, the instantaneous scattering images (Fig. 4) seem to show an interface approximating the instantaneous outer edge of the mixing layer, and this difference is reflected in the mean profiles.

The profile of the standard deviation of the scattering intensity is compared to the hot-wire data of Hayakawa et al.[28] in Fig. 7. The standard deviation of the mass flux is plotted along with the standard deviation of the density, derived from the mass flux data by applying the strong Reynolds analogy (see Spina[29] and Smith and Smits[30]).

The fluctuation intensity profiles peak at approximately the same location [$(y - y_0)/\delta \approx 0.6$] and have similar behavior toward the

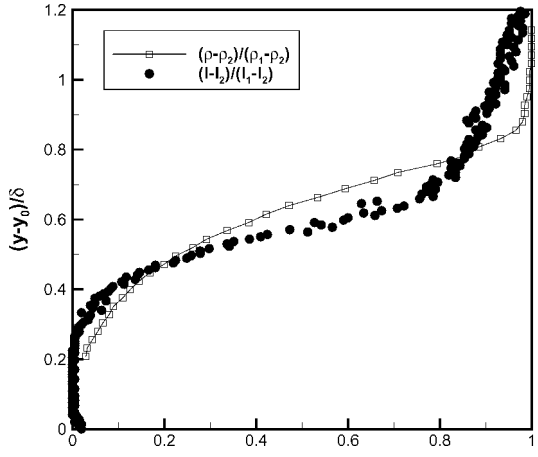

Fig. 6 Mean profiles through shear layer derived from side-view images.

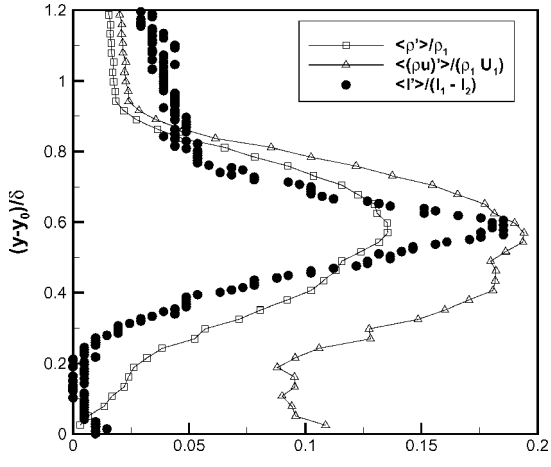

Fig. 7 From side-view images, rms profiles through shear layer.

outer edge of the turbulent mixing layer. There is a relatively low intensity of scattering fluctuations toward the low-speed side of the turbulent mixing layer due to the lack of scattering particles in that region. In contrast, data obtained by Elliott et al.[12] using the product formation method show another local maximum in the rms scattering intensity profiles on the low-speed side of two turbulent mixing layer flows (nominal $M_c = 0.51$ and 0.86).

Spatial Correlations

A spatial correlation function was calculated over a set of images between the scattering intensity recorded at each pixel in the field of view and the scattering intensity at a reference location. The correlation coefficient was defined as

$$R(\boldsymbol{x}, \boldsymbol{r}) = \frac{\sum_{i=1}^{N} [I_i(\boldsymbol{x}) - \bar{I}][I_i(\boldsymbol{x}+\boldsymbol{r}) - \bar{I}]}{\sqrt{\sum_{i=1}^{N} [I_i(\boldsymbol{x}) - \bar{I}]^2 \sum_{i=1}^{N} [I_i(\boldsymbol{x}+\boldsymbol{r}) - \bar{I}]^2}} \tag{4}$$

where I is the intensity of scattered light recorded by the video camera, $\boldsymbol{x}$ is a reference location, and $\boldsymbol{r}$ is a relative displacement vector. Previous work applying these two-point correlations to flow visualization[24,31] of Mach 2.5 and Mach 2.9 turbulent boundary layers has shown good agreement with hot-wire cross-correlation data.[32,33]

The correlation analysis was applied to side- and plan-view images of the free shear layer. All of the correlations were calculated with a sample size of 200 images with a resolution of 640×480 pixels.

Figure 8 shows selected correlation plots for the side-view images of the flow, calculated for reference points located 25.1, 25.6, 26.2, and 26.8 mm from the floor of the cavity of the experimental model [$(y_r - y_0)/\delta = 0.44$, 0.49, 0.55, and 0.60]. The horizontal position of the reference point was held constant at the center of the field of view. (Note that only a portion of the field of view present in the raw data, as in Fig. 4, is shown.)

With the reference point near the outer edge of the visualized shear layer (Fig. 8a), the area enclosed by a given correlation contour is relatively small, reflecting the tops of the structures that occasionally penetrate into the freestream (Fig. 4). As the reference point approaches the center of the shear layer, the correlation contours enclose a progressively larger area (Figs. 8b and 8c), responding to the large-scale bulges observed in the instantaneous images of the shear layer. The contours are seen to be roughly elliptical in shape, with the primary axis oriented at approximately 45 deg from the streamwise direction. As an indication of the mean length scale of the structures, the principal axes of the $R = 0.75$ correlation contour are 1.7 and 1.1 mm long (0.16δ by 0.10δ) for a reference point located at a height of 26.8 mm or $(y - y_0)/\delta = 0.60$.

Because the correlation contours are approximately elliptical in shape, the orientation of the major axis of a correlation contour provides an indication of the average inclination of a large-scale structure. The structure angle was determined graphically from the correlation plots by measuring the angle between the primary axis of the $R = 0.75$ correlation contour and the streamwise direction. Figure 9 is a plot of structure angle vs normalized height in the shear layer.

For reference points located between $0.40 \leq (y - y_0)/\delta \leq 0.60$, the structure angle was found to be 40–50 deg, and to decrease with height in the mixing layer. These results most likely represent the backs of the δ-scale bulges in the shear layer. Results are not shown for reference points located outside of this range because the structure angle was found to be poorly defined due to a lack of resolution in the flow visualization data.

Shau and Dolling[34] have obtained comparable structure angles in a $M_c = 0.3$ shear layer using both schlieren photography and cross correlations of pitot pressure fluctuations. The present results also agree well with the Mie scattering results obtained by Elliott et al.[12] in turbulent mixing layers at $M_c = 0.51$ and 0.86. The structure angle profile computed here is quite similar in shape to the corresponding profiles in a Mach 2.9 turbulent boundary layer obtained by Poggie[24] using the current method and by Spina[29] using cross correlations of vertically separated hot wires.

The correlation analysis was also carried out for the plan-view images with the reference point located at the center of the field of view. The results are shown in Fig. 10. [Note that only a portion of the field of view present in the raw data (Fig. 5) is shown.] The correlation contours have a shape similar to an ellipse, with the major axis aligned with the flow direction. The region enclosed by the $R = 0.75$ contour has principal axes of length 3.3 and 2.2 mm (0.26δ by 0.19δ). These results reflect the streamwise elongation of the structures observed in the flow.

Double-Pulse Experiments

A series of experiments was conducted in which the Nd:YAG laser was configured to fire twice in rapid succession. Two cameras were positioned on opposite sides of the wind tunnel (Fig. 11) and gated so that each recorded one of the two sequential laser pulses. As shown in Fig. 11b, a structure observed by camera 1 during the first laser pulse would convect downstream during the interval between pulses and be recorded during the second pulse within the field of view of camera 2. The two fields of view were displaced in the streamwise direction to allow longer time delays to be used without increasing the size of the camera fields of view.

The fields of view were 28.6 mm wide by 21.4 mm high and had identical size and vertical position to within 0.1 mm. The bottom edge of the images was 18.4 mm off the floor of the cavity of the experimental model, and the first field began 37.0 mm downstream of the backward-facing step in the experimental model (Fig. 1).

To avoid systematic error in the measurements of the convection velocity, three independent measurements were made of the streamwise offset between the two fields of view. First, before the set of wind-tunnel runs, a precision grid was placed in the tunnel aligned with the laser sheet. The offset was measured from the

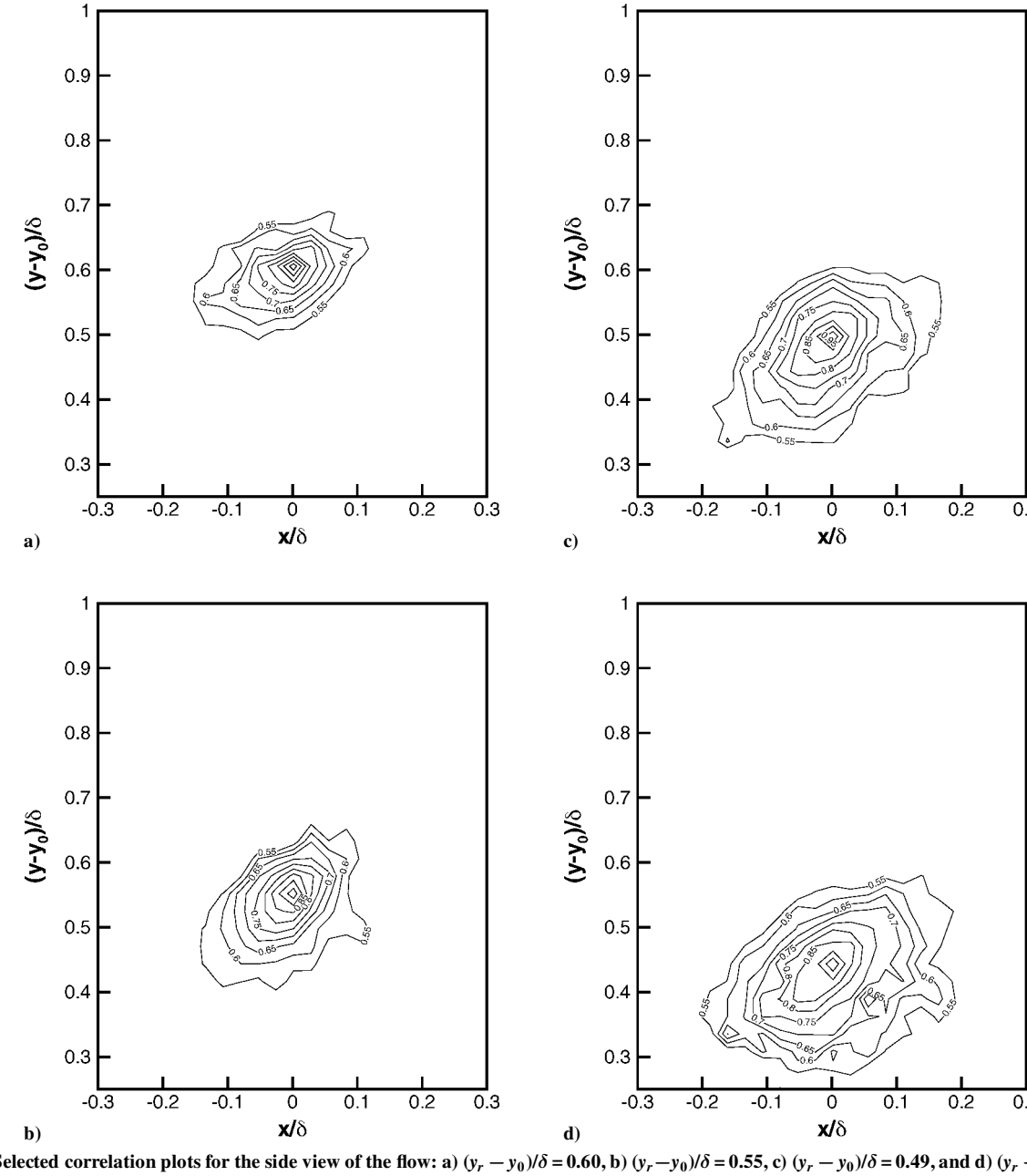

Fig. 8 Selected correlation plots for the side view of the flow: a) $(y_r - y_0)/\delta = 0.60$, b) $(y_r - y_0)/\delta = 0.55$, c) $(y_r - y_0)/\delta = 0.49$, and d) $(y_r - y_0)/\delta = 0.44$.

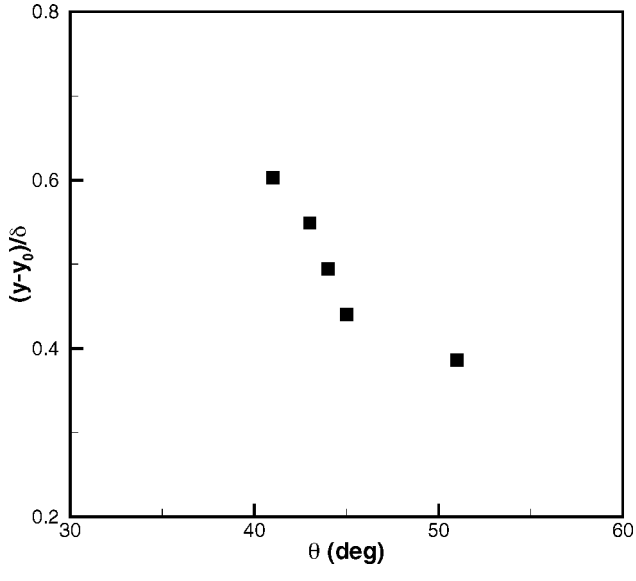

Fig. 9 Structure angle vs position in the shear layer.

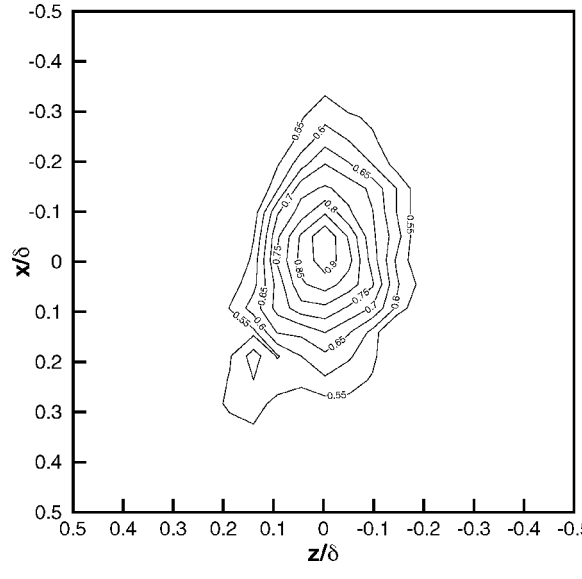

Fig. 10 Correlation plot for the plan view of the shear layer.

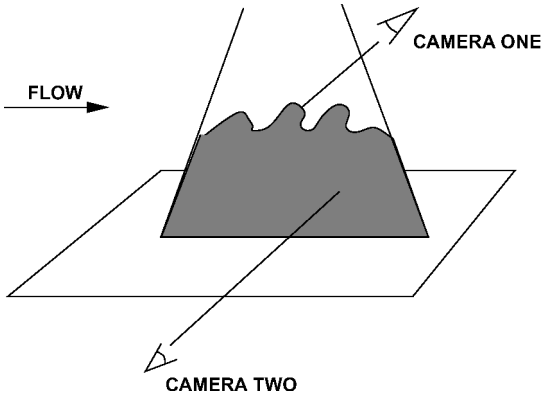

a) Configuration of cameras

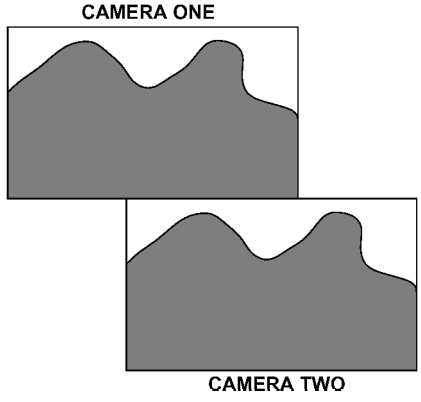

b) Resulting fields of view

Fig. 11 Experimental setup for double-pulse laser scattering experiments.

images recorded with the two cameras. Second, before each wind-tunnel run, a portion of the laser sheet was blocked with a card, and the position of the edge of the resulting shadow was recorded with both cameras. Finally, data were obtained with zero time delay (single-pulse mode) and correlated to obtain the offset of the fields of view. The three measurements indicated that the displacement was 12.1 ± 0.2 mm.

Pitot probe surveys[22] indicate that the shear layer thickness varies between 7.4 and 11.4 mm over the field of view covered by the two cameras together. For reference, the shear layer parameters at a station 63.5 mm downstream of the backward-facing step will be used: $\delta = 9.4$ mm and $y_0 = 21.3$ mm. In terms of these parameters, the individual fields of view were 3.0δ wide by 2.3δ high, and the offset in the fields of view was $(1.27 \pm 0.02)\delta$. The nondimensional time delays ($U_1\tau/\delta$) were 1.64 and 2.12, where U_1 is the freestream velocity (591 m/s for a stagnation temperature of 280 K). The images show heights within the shear layer in the range $-0.31 \leq (y - y_0)/\delta \leq 1.97$.

Qualitative Results

An initial test was made with the laser running in single-pulse mode (zero time delay). Figure 12 shows an example of the results. The image from Camera One was reversed so that the flow direction would appear as left to right, and the images were offset in Fig. 12 so that corresponding streamwise locations coincided. The strong correspondence between the two images indicates that the magnification and sensitivity of the two cameras were well matched.

A second test was made with a 26.1-μs time delay between laser pulses. An example is shown in Fig. 13. Structures are seen to have traveled downstream in the time between pulses. Furthermore, smaller scale structures appear to form on the back of the large-scale bulges in the mixing layer. Growth of smaller scale structures on the backs of large-scale bulges has been observed using similar experimental techniques by Cogne et al.[35] and by Smith[31] in a Mach 2.9 turbulent boundary layer.

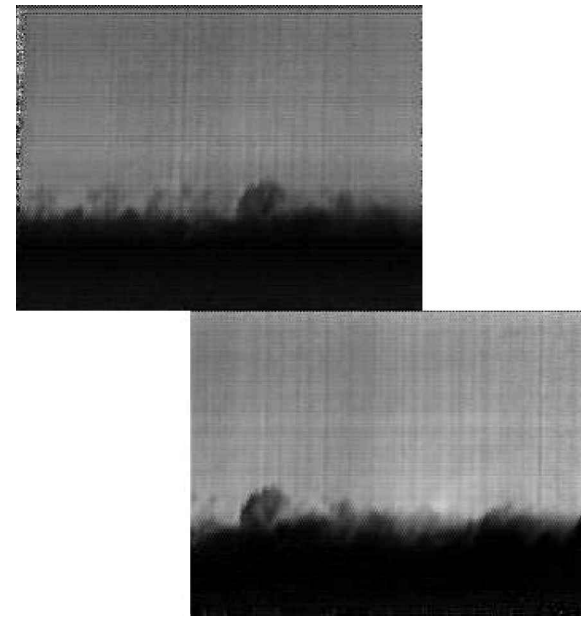

Fig. 12 Data taken with zero time delay; top, camera 1 and bottom, camera 2.

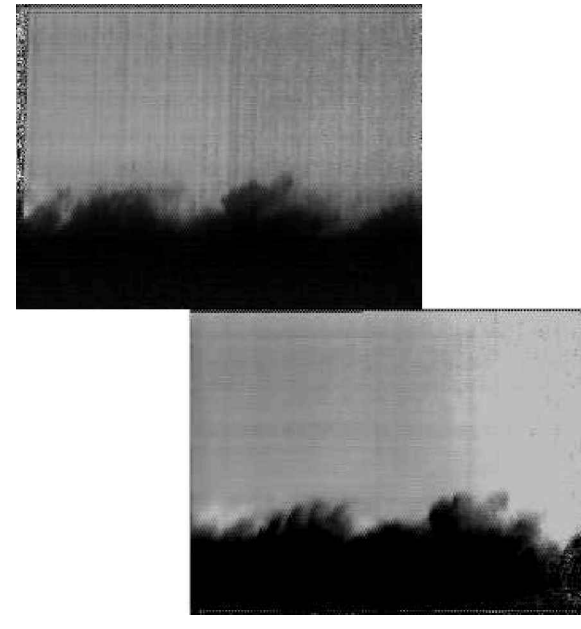

Fig. 13 Data taken with a time delay of 26.1 μs; top, camera 1 and bottom, camera 2; flow left to right.

Figure 14 shows a pair of example images with a 33.7-μs time delay. The structures have traveled farther downstream in this case, and appear to have evolved somewhat more during the greater time delay.

Convection Velocity

A spatial correlation function was used to identify horizontal motion of structures in pairs of sequential images from the double-pulse Rayleigh scattering experiments. The data were normalized to have zero mean and unit standard deviation, and the spatial cross-correlation was defined as

$$R(x, y) = \begin{cases} \dfrac{1}{L - x} \displaystyle\int_0^{L-x} I_A(\xi, y) I_B(\xi + x, y)\, \mathrm{d}\xi, & x \geq 0 \\ \dfrac{1}{L - |x|} \displaystyle\int_{|x|}^{L} I_A(\xi, y) I_B(\xi + x, y)\, \mathrm{d}\xi, & x \leq 0 \end{cases} \quad (5)$$

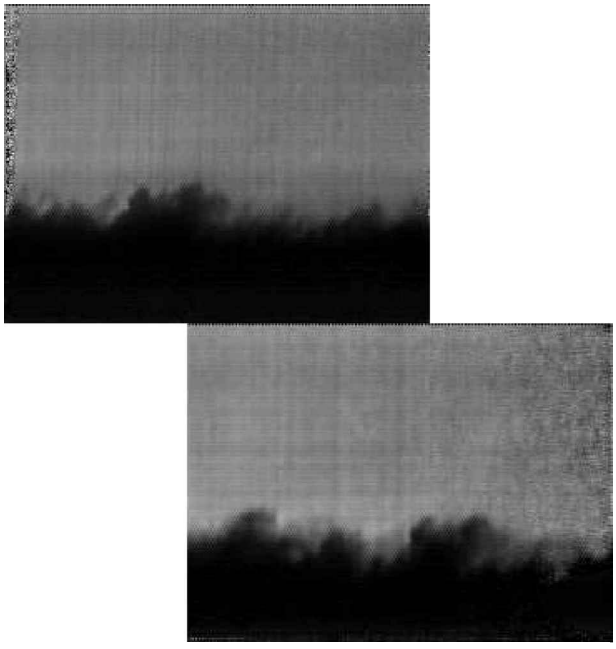

Fig. 14 Data taken with a time delay of 33.7 μs; top, camera 1 and bottom, camera 2; flow left to right.

where x is the horizontal displacement, y is a fixed height in the shear layer, L is the width of the field of view, and I_A and I_B represent intensity of scattered light recorded in the pair of images to be correlated. The computer program used for the calculations is described in Ref. 8.

The double-pulse Rayleigh scattering images were analyzed in sets of 50 images with a resolution of 512×384 pixels. Each row was zero padded to 1024 pixels to allow for the wraparound effect of the computational algorithm. For each pair of sequential images of the flow, Eq. (5) was applied to each pair of corresponding rows in turn, and then the correlations for the individual images were averaged. The streamwise displacement with maximum correlation was identified for each height within the shear layer and used to estimate the streamwise component of the convection velocity as follows:

$$U_c = \ell/\tau \tag{6}$$

where ℓ is the displacement for maximum correlation and τ is the time delay between laser pulses.

Using a standard error propagation analysis, the uncertainty in the calculation of the convection velocity can be estimated as

$$|\delta U_c/U_c| \leq |\delta\ell/\ell| + |\delta\tau/\tau| \tag{7}$$

where δU_c is the uncertainty in the convection velocity, $\delta\ell$ is the uncertainty in the displacement, and $\delta\tau$ is the uncertainty in the time delay. There are several possible sources of random error in determining the displacement ℓ for maximum correlation: uncertainty in positioning the calibration grid and the laser sheet on the centerline of the wind tunnel, vibration of the cameras during a wind tunnel run, and uncertainty in locating the peak in the correlation curve. Thus, a conservative estimate of the uncertainty in the displacement would be 7%, for example, 1.0 mm in 14 mm. The uncertainty in the time delay is approximately 2%, for example, 0.5 μs in 26 μs. Thus the overall error in the computed convection velocity is expected to be less than 9%.

An additional consideration in evaluating the uncertainty in the convection velocity measurement is the large separation in space and time between the sequential measurements. Because the nondimensional time between measurements ($U_1\tau/\delta$) was on the order of two, only the largest scale and longest lived structures in the shear layer turbulence are identified in the present measurement.

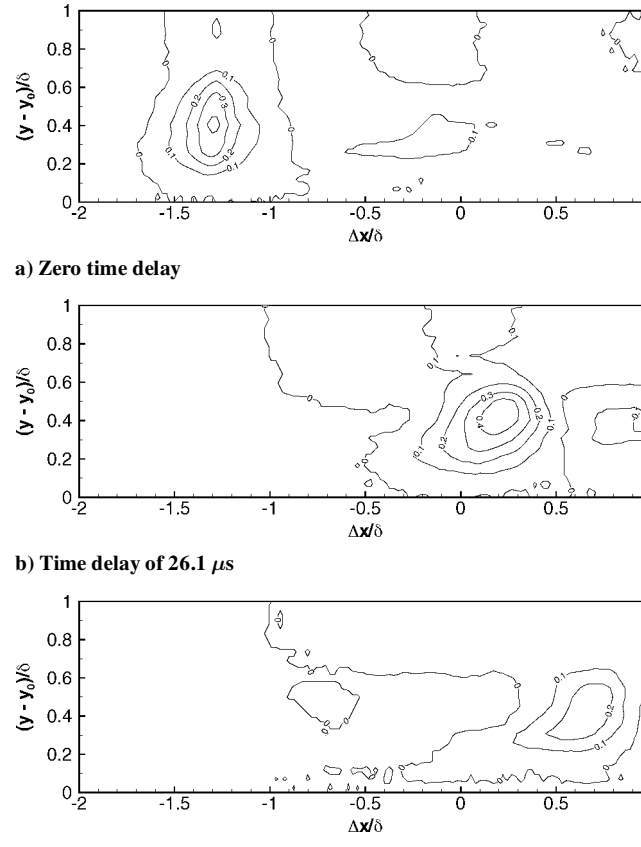

a) Zero time delay

b) Time delay of 26.1 μs

c) Time delay of 33.7 μs

Fig. 15 Line-by-line correlation plots.

Figure 15 shows line-by-line correlations for the three time delays; each of Figs. 15a–15c is an average of the correlation of 50 pairs of images. The vertical axis represents the height within the shear layer, and the horizontal axis represents the relative displacement between pairs of images. Figure 15a shows the case with zero time delay. There is a clear correlation of the features within the region representing the visible shear layer. The maximum correlation for each height is located at the same streamwise displacement, which corresponds to the streamwise offset between the two fields of view ($\Delta x = -12.1$ mm and $\Delta x/\delta = -1.29$). The correlations in Fig. 15b for the 26.1-μs time delay have maxima that lie along a diagonal line, indicating the profile of convection velocity in the shear layer. Figure 15c shows the case with a 33.7-μs time delay; here the displacement for maximum correlation has increased due to the greater time delay. The convection velocity profile is also evident in this case, even though the level of correlation has decreased with the increased time delay.

Figure 16 shows, for each time delay, the correlation coefficient vs the relative displacement of the pair of images at a height of 25.3 mm above the floor of the cavity in the experimental model [$(y - y_0)/\delta = 0.43$]. The peak correlation is seen to decrease as the time delay increases due to the evolution of the turbulence structures. The correlation profile for the single-pulse (zero time delay) case is somewhat distorted and has a lower maximum than expected because a relatively small portion of each pair of images overlaps for the displacements of interest in this case. The close agreement of the location of the peak correlation in the single-pulse data with the offset in the fields of view measured from the calibration grid is clear in Fig. 16.

The convection velocity calculated from Eq. (6) for each height in the shear layer is plotted in Fig. 17. A mean velocity profile, obtained from probe surveys[22] at a station 63.5 mm downstream of the backward-facing step, is included in Fig. 17 for reference. There is good agreement between the data taken at the two time delays, and there is relatively little scatter in the data. The convection velocity varies between $0.82U_1$ and $0.95U_1$ over a range of about 0.4δ in the

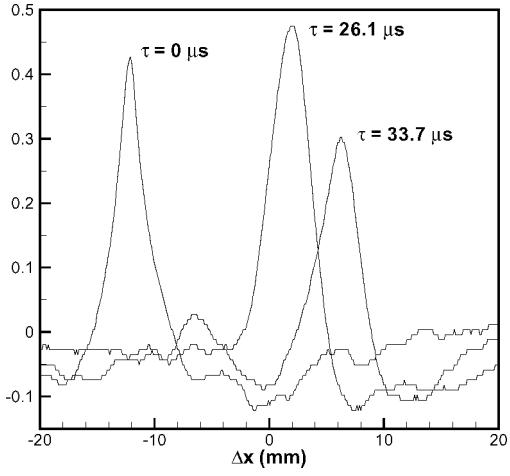

Fig. 16 Correlation vs displacement at a height of 25.3 mm or $(y - y_0)/\delta = 0.43$ for each of the three time delays.

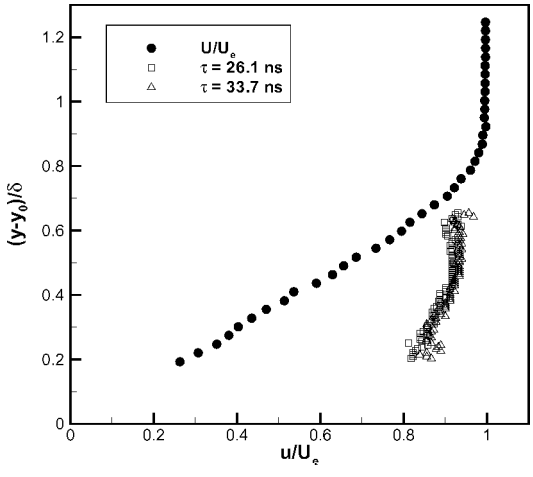

Fig. 17 Convection velocity profile for free shear layer.

center part of the shear layer. (For comparison, a convection velocity of $0.84U_e$ was obtained from pressure transducer measurements in the ramp boundary-layer flow just downstream of shear layer reattachment.[5])

Whereas the isentropic model of Bogdanoff[15] predicts a uniform convective Mach number of $M_c = (U_1 - U_2)/(a_1 + a_2) = 1.1$ throughout the shear layer, the present results indicate that the convective Mach number, defined by Eq. (1), is about 1.6 relative to the low-speed side of the shear layer and about 0.3 relative to the high-speed side. These data follow the same trend as Papamoschou's measurements[19] of the convection velocity in two-stream mixing layers using a two-spark schlieren system. Papamoschou found that the convection velocity was essentially uniform across the shear layer under a variety of flow conditions and that, at high nominal convective Mach numbers, the true convective Mach number tended to be supersonic on one side of the shear layer and subsonic on the other side. In other words, the convection velocity tended to approach that of the high-speed freestream for these cases.

The data reported in Ref. 19 were replotted in Fig. 18 with the measured convective Mach number on each side of the shear layer shown as a function of the nominal convective Mach number. Rather than following the isentropic model (marked as a solid line in Fig. 18) Papamoschou's data fall onto two curves: one roughly constant at subsonic Mach number and the other rapidly increasing with the nominal convective Mach number. The present results fall nicely on the two curves. These results are consistent with the observation of shock waves in the present flow and tend to support the idea that the isentropic model breaks down in shear layers with strong compressibility effects.

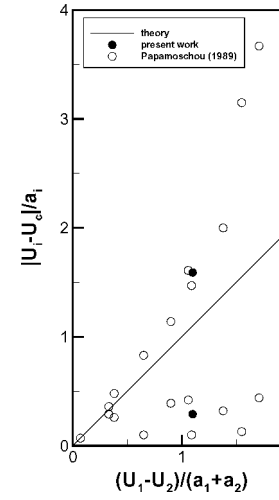

Fig. 18 Measured convective Mach numbers relative to the two streams compared to the isentropic model.

Conclusions

An experimental study was made of a flow in which a turbulent boundary layer separates at a backward-facing step, forms a free shear layer over a cavity, and reattaches on a ramp downstream. A flow visualization technique based on Rayleigh scattering from nanometer-scale contaminant particles was applied to the self-similar portion of the turbulent mixing layer at a nominal convective Mach number of 1.1. The interface marked by the vaporization of the particles revealed the large-scale organized turbulence structures in the mixing layer. Measurements of the length scale, speed, and orientation of the coherent structures were derived from the flow visualization data and were found to agree well with conventional point probe measurements as well as the results of other flow visualization studies of mixing layers. As has been found in other experimental studies of planar mixing layers,[12,19] the measured convection velocity varied moderately across the mixing layer, and the convective Mach number derived from direct measurements of the convection velocity did not agree with the prediction of the isentropic model.[15,16]

For unconfined separated flows, and for cavity flows at relatively high convective Mach number, the primary mechanism for unsteadiness near reattachment appears to be perturbation by organized structures in the incoming turbulent flow.[3–5] For the present flow, the spectrum of the wall pressure fluctuations near reattachment was found to scale on the characteristic length and convection velocity of organized structures in the incoming free shear layer (Fig. 2 and Ref. 5). Accurate characterization of the mixing layer turbulence is important given this strong link between large-scale organized structures and intense unsteadiness at reattachment. The present results, along with previously published probe surveys, demonstrate that the flow over the cavity is essentially equivalent to a standard planar mixing layer flow and, thus, forms a well-characterized initial condition for the reattachment flow downstream. In combination with our previous study,[5] the present results add insight into cavity flow unsteadiness for the case where the driving mechanism is related to broadband turbulent fluctuations, rather than discrete acoustic resonances.

Acknowledgments

This work was funded in part by grants from the Air Force Office of Scientific Research and NASA Langley Research Center. Technical support was provided by R. Bogart and W. Stokes. J. Forkey and R. Miles provided advice in the design and execution of the laser diagnostics experiments. The first author is indebted to R. Kimmel and A. Creese for valuable discussions of this work.

References

[1] Rossiter, J. E., "Wind Tunnel Experiments on the Flow over Rectangular Cavities at Subsonic and Transonic Speed," Repts. and Memoranda 3488, British Aeronautical Research Council, London, Oct. 1964.

[2]Rizzetta, D. P., and Visbal, M. R., "Large-Eddy Simulation of Supersonic Cavity Flowfields Including Flow Control," *AIAA Journal*, Vol. 41, No. 8, 2003, pp. 1452–1462.

[3]Ünalmis, Ö. H., Clemens, N. T., and Dolling, D. S., "Experimental Study of Shear-Layer/Acoustics Coupling in Mach 5 Cavity Flow," *AIAA Journal*, Vol. 39, No. 2, 2001, pp. 242–252.

[4]Murray, R. C., and Elliott, G. S., "Characteristics of the Compressible Shear Layer over a Cavity," *AIAA Journal*, Vol. 39, No. 5, 2001, pp. 846–856.

[5]Poggie, J., and Smits, A. J., "Shock Unsteadiness in a Reattaching Shear Layer," *Journal of Fluid Mechanics*, Vol. 429, 2001, pp. 155–185.

[6]Smith, K. M., and Dutton, J. C., "Investigation of Large-Scale Structures in Supersonic Planar Base Flows," *AIAA Journal*, Vol. 34, No. 6, 1996, pp. 1146–1152.

[7]Wu, P., Lempert, W. R., and Miles, R. B., "Megahertz Pulse-Burst Laser and Visualization of Shock-Wave/Boundary-Layer Interaction," *AIAA Journal*, Vol. 38, No. 4, 2000, pp. 672–679.

[8]Poggie, J., "On the Control of a Compressible, Reattaching Shear Layer," Ph.D. Dissertation, Dept. of Mechanical and Aerospace Engineering, Princeton Univ., Princeton, NJ, Jan. 1995.

[9]Brown, G. L., and Roshko, A., "On Density Effects and Large Structure in Turbulent Mixing Layers," *Journal of Fluid Mechanics*, Vol. 64, 1974, pp. 775–816.

[10]Lasheras, J. C., and Choi, H., "Three-Dimensional Instability of a Plane Free Shear Layer: An Experimental Study of the Formation and Evolution of Streamwise Vortices," *Journal of Fluid Mechanics*, Vol. 189, 1988, pp. 53–86.

[11]Ashurst, W. T., and Meiburg, E., "Three-Dimensional Shear Layers via Vortex Dynamics," *Journal of Fluid Mechanics*, Vol. 189, 1988, pp. 87–116.

[12]Elliott, G. S., Samimy, M., and Arnette, S. A., "The Characterisitcs and Evolution of Large-Scale Structures in Compressible Mixing Layers," *Physics of Fluids*, Vol. 7, 1995, pp. 864–876.

[13]Clemens, N. T., and Mungal, M. G., "Two- and Three-Dimensional Effects in the Supersonic Mixing Layer," *AIAA Journal*, Vol. 30, No. 4, 1992, pp. 973–981.

[14]Elliott, G. S., Samimy, M., and Arnette, S. A., "Study of Compressible Mixing Layers Using Filtered Rayleigh Scattering Based Visualizations," *AIAA Journal*, Vol. 30, No. 10, 1992, pp. 2567–2569.

[15]Bogdanoff, D. W., "Compressibility Effects in Turbulent Free Shear Layers," *AIAA Journal*, Vol. 21, 1983, pp. 926, 927.

[16]Papamoschou, D., and Roshko, A., "The Compressible Turbulent Shear Layer: An Experimental Study," *Journal of Fluid Mechanics*, Vol. 197, 1988, pp. 453–477.

[17]Barre, S., Quine, C., and Dussauge, J. P., "Compressibility Effects on the Structure of Supersonic Mixing Layers: Experimental Results," *Journal of Fluid Mechanics*, Vol. 259, 1994, pp. 47–78.

[18]Smits, A. J., and Dussauge, J.-P., *Turbulent Shear Layers in Supersonic Flow*, 1st ed., American Inst. of Physics, Woodbury, NY, 1996, Sec. 6.3, pp. 138–141.

[19]Papamoschou, D., "Structure of the Compressible Turbulent Shear Layer," *AIAA Journal*, Vol. 29, 1991, pp. 680, 681.

[20]Bogdonoff, S. M., "The Design, Construction, and Operation of the Princeton 4 by 8 Inch Variable-Density Supersonic Tunnel," TR 34, Project Squid, Princeton Univ., Princeton, NJ, Oct. 1951.

[21]Vas, I. E., and Bogdonoff, S. M., "A Preliminary Report on the Princeton University High Reynolds Number 8 in × 8 in Supersonic Tunnel," Gas Dynamics Lab., Internal Memorandum 39, Princeton Univ., Princeton, NJ, Oct. 1971.

[22]Baca, B. K., "An Experimental Study of the Reattachment of a Free Shear Layer in Compressible Turbulent Flow," M.S. Thesis, Dept. of Mechanical and Aerospace Engineering, Princeton Univ., Princeton, NJ, Sept. 1981.

[23]Horstman, C. C., Settles, G. S., Williams, D. R., and Bogdonoff, S. M., "A Reattaching Free Shear Layer in Compressible Turbulent Flow," *AIAA Journal*, Vol. 20, 1982, pp. 79–85.

[24]Poggie, J., "Quantitative Flow Visualization Applied to the Study of Compressible Turbulent Flow," M.S. Thesis, Dept. of Mechanical and Aerospace Engineering, Princeton Univ., Princeton, NJ, June 1991.

[25]Shirinzadeh, B., Hillard, M. E., and Exton, R. J., "Condensation Effects on Rayleigh Scattering Measurements in a Supersonic Wind Tunnel," *AIAA Journal*, Vol. 29, 1991, pp. 242–246.

[26]Poggie, J., "Quantitative Visualization of Supersonic Flow Using Rayleigh Scattering," AIAA Paper 96-0436, Jan. 1996.

[27]Settles, G. S., Baca, B. K., Williams, D. R., and Bogdonoff, S. M., "Reattachment of a Compressible Turbulent Free Shear Layer," *AIAA Journal*, Vol. 20, 1982, pp. 60–67.

[28]Hayakawa, K., Smits, A. J., and Bogdonoff, S. M., "Turbulence Measurements in a Compressible Reattaching Shear Layer," *AIAA Journal*, Vol. 22, 1984, pp. 889–895.

[29]Spina, E. F., "Organized Structures in a Supersonic Turbulent Boundary Layer," Ph.D. Dissertation, Dept. of Mechanical and Aerospace Engineering, Princeton Univ., Princeton, NJ, Oct. 1988.

[30]Smith, D. R., and Smits, A. J., "Simultaneous Measurement of Velocity and Temperature Fluctuations in the Boundary Layer of a Supersonic Flow," *Experimental Thermal and Fluid Science*, Vol. 7, 1993, pp. 221–229.

[31]Smith, M. W., "Flow Visualization in Supersonic Turbulent Boundary Layers," Ph.D. Dissertation, Dept. of Mechanical and Aerospace Engineering, Princeton Univ., Princeton, NJ, Oct. 1989.

[32]Spina, E. F., and Smits, A. J., "Organized Structures in a Compressible Turbulent Boundary Layer," *Journal of Fluid Mechanics*, Vol. 182, 1987, pp. 85–109.

[33]Spina, E. F., Donovan, J. F., and Smits, A. J., "On the Structure of High-Reynolds-Number Supersonic Turbulent Boundary Layers," *Journal of Fluid Mechanics*, Vol. 222, 1991, pp. 293–327.

[34]Shau, Y. R., Dolling, D. S., and Choi, K. Y., "Organized Structure in a Compressible Turbulent Shear Layer," *AIAA Journal*, Vol. 31, No. 8, 1993, pp. 1398–1405.

[35]Cogne, S., Forkey, J., Lempert, W., Miles, R. B., and Smits, A. J., "Evolution of Large-Scale Structures in a Supersonic Turbulent Boundary Layer," *Transitional and Turbulent Compressible Flows*, FED-Vol. 151, American Society of Mechanical Engineers, Fairfield, NJ, 1993, pp. 229–237.

W. Dahm
Associate Editor